

N64-25773

CODE 1

CAT. 10

NASA CR-56969

20P

Technical Report No. 32-620

Hypervelocity Shock Tube

*Daniel J. Collins
Floyd R. Livingston
Terry L. Babineaux
Norman R. Morgan*



JET PROPULSION LABORATORY
CALIFORNIA INSTITUTE OF TECHNOLOGY
PASADENA, CALIFORNIA

June 15, 1964

OTS PRICE

XEROX \$ 1.60 ph

MICROFILM \$ _____

Technical Report No. 32-620

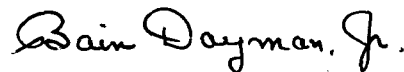
Hypervelocity Shock Tube

Daniel J. Collins

Floyd R. Livingston

Terry L. Babineaux

Norman R. Morgan



Bain Dayman, Jr., Chief
Aerodynamic Facilities Section

JET PROPULSION LABORATORY
CALIFORNIA INSTITUTE OF TECHNOLOGY
PASADENA, CALIFORNIA

June 15, 1964

Copyright © 1964
Jet Propulsion Laboratory
California Institute of Technology

Prepared Under Contract No. NAS 7-100
National Aeronautics & Space Administration

CONTENTS

I. Introduction	1
II. Physical Description	2
A. Driven Tube	2
B. Driver	2
C. Capacitor Bank	4
D. Vacuum System	5
III. Basic Instrumentation	6
A. Initial-Pressure System (Driven Tube)	6
B. Shock-Speed Determination	6
C. Model Support and Instrument Ports	8
IV. Operation	9
V. Performance and Evaluation	10
VI. Summary	13
References	13

FIGURES

1. Shock tube assembly	2
2. Shock tube and related systems	3
3. Driver schematic	3
4. Capacitor bank	4
5. Voltage and amperage characteristics of capacitor bank	4
6. Control console	5
7. Vacuum system schematic	5
8. Low-pressure measuring system	6
9. Photomultiplier trace	7
10. Block diagram of shock-speed measuring system	7
11. Raster trace	7
12. Sketch of instrument port	8

FIGURES (Cont'd)

13. Model support	8
14. Driver pressure vs energy input	10
15. Driver temperature vs energy input	10
16. Sound-speed ratio vs energy input	11
17. Shock speed vs energy input	11
18. Shock-speed attenuation	11
19. Test time vs shock speed (250 μ)	12
20. Test time vs shock speed (1 mm)	12
21. Image-converter-camera photograph of shock wave	12

ABSTRACT

25 773

The design and performance of the Jet Propulsion Laboratory's hypervelocity 6-in. shock tube are described. The facility is capable of simulating planetary entry velocities of 45,000 fps. Shock velocities of 32,000 fps into 0.250 mm Hg of air have been achieved in the 6-in. tube, with a useful test time of 12 μ sec. Investigations of convective heat transfer and radiant heat transfer have been completed.

Author

I. INTRODUCTION

In the field of planetary-entry fluid physics, present interplanetary missions require that research equipment have the ability to simulate space-probe entry velocities up to 42,000 fps. The Jet Propulsion Laboratory (JPL) has a need to investigate high-temperature gasdynamic effects in planetary atmospheres. Some of the practical engineering problems are connected with the design of the spacecraft's heat shield, thus requiring a knowledge

of convective heat transfer, equilibrium radiation heat transfer, and nonequilibrium radiation heat transfer.

The JPL hypervelocity shock tube has been constructed to meet these needs. An electric shock tube (Refs. 1 and 2) was selected, since the electrical-discharge approach had already proved successful in obtaining the desired velocity simulation.

An electrical shock tube is similar to a normal shock tube, except that a high-temperature, high-pressure reservoir is created behind the shock tube diaphragm by

means of an electrical discharge in the driver gas. This Report describes in detail the performance and capabilities of the JPL electrical shock tube.

II. PHYSICAL DESCRIPTION

A. Driven Tube

Figure 1 presents a schematic of the entire shock tube. The driven tube is a stainless steel tube, 6 in. in internal diameter, with a wall thickness of $\frac{3}{8}$ in. and an interior finish of 15μ . The overall length of the driven tube is approximately 43 ft. The instrument ports are mounted flush with the interior surface of the tube. The steps at the flange joints are less than ± 0.0005 in.

The transition section from the driver to the driven tube incorporates a square-to-round transition with a simple conical expansion to the 6-in. diameter. The tube is fastened to the building foundation at the transition

section. A photograph of the shock tube and related systems is presented in Fig. 2.

B. Driver

In Fig. 3, the schematic of the driver also shows in detail the cable connection from the capacitor bank. The driver has a 2-in. inside diameter and is 26 in. long. The Teflon liner used to insulate the discharge region and insure an axial arc reduces the usable diameter to $1\frac{3}{8}$ in.

The ignition wire is attached to a spider which prevents the arc from impinging on the diaphragm. A nylon spacer

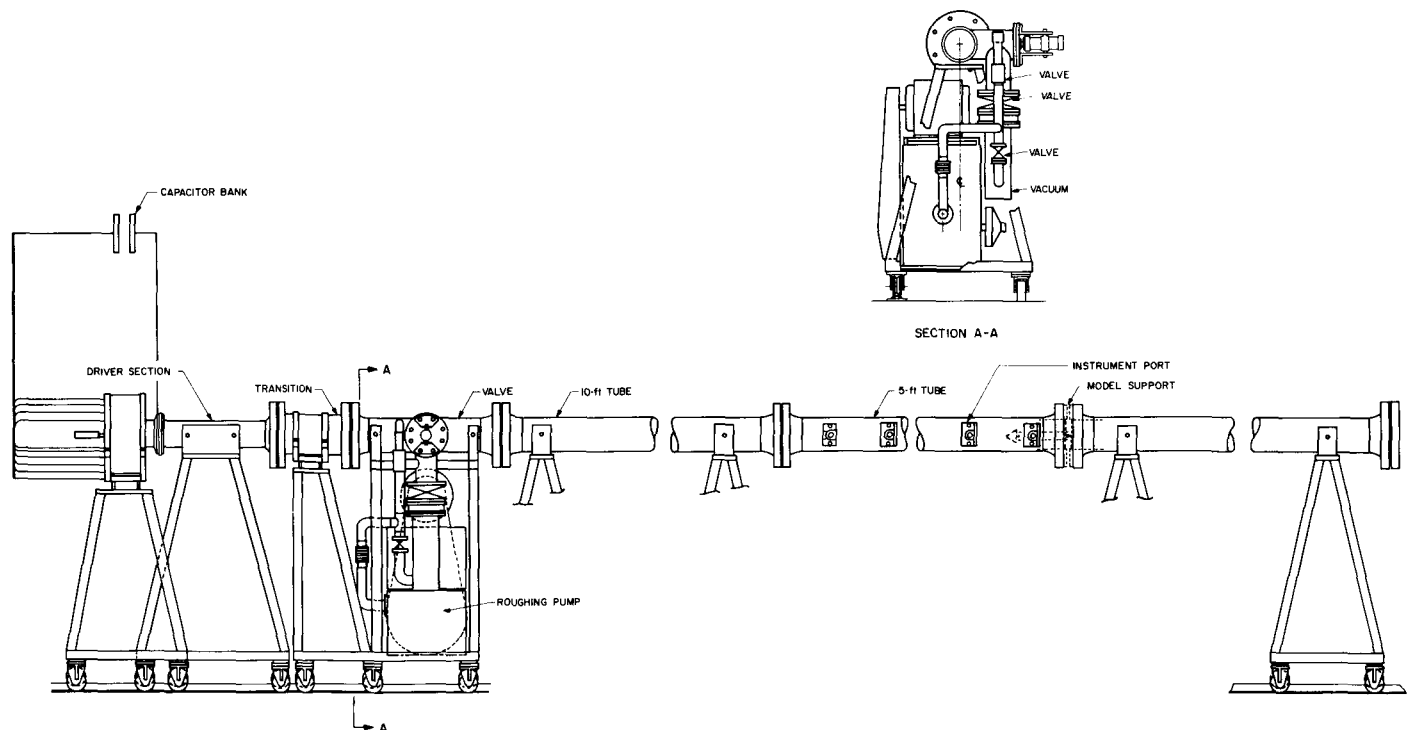


Fig. 1. Shock tube assembly

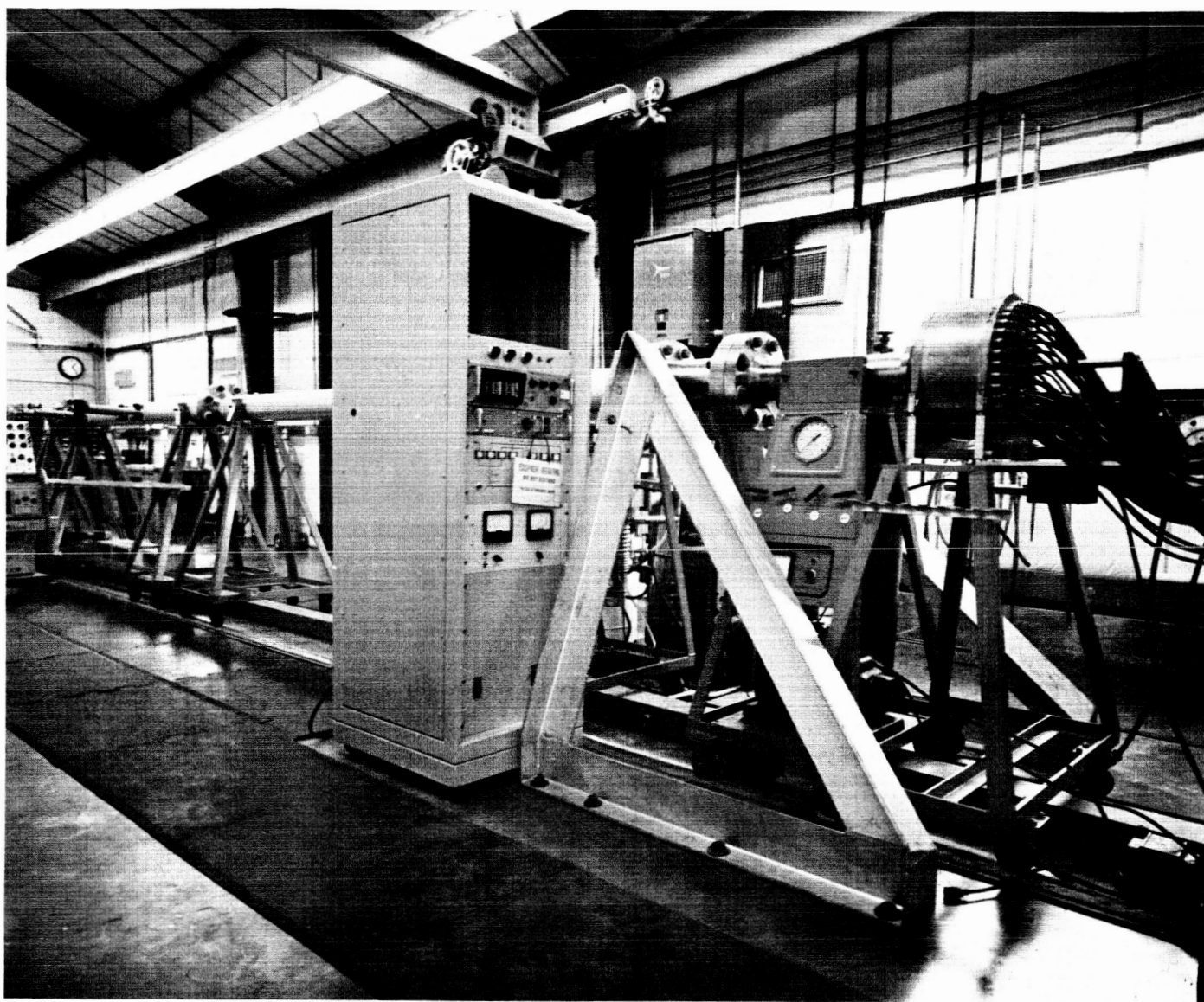


Fig. 2. Shock tube and related systems

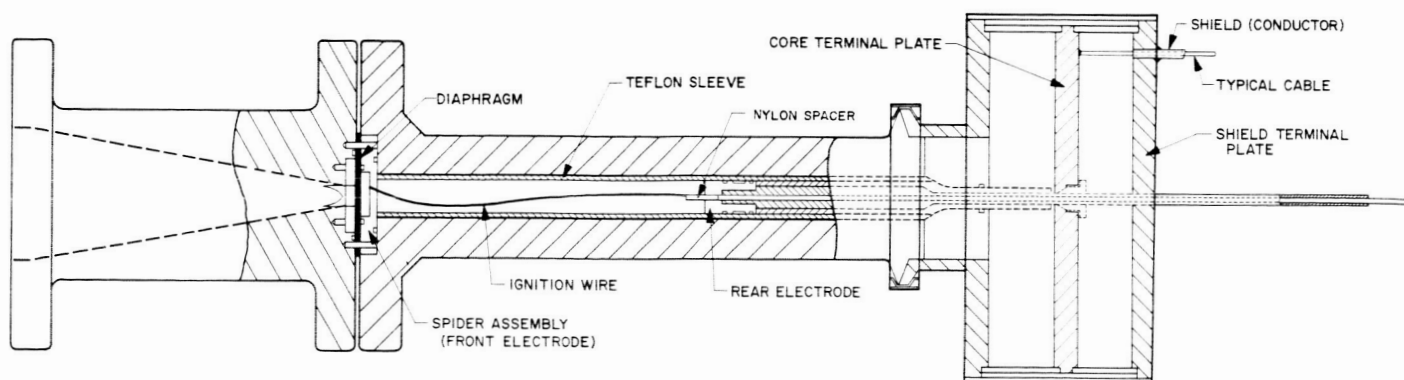


Fig. 3. Driver schematic

prevents the ignition wire from touching the rear electrode during the charging period. To initiate the electrical discharge, a solenoid draws the wire back, and contact is made with the rear electrode. A 10-mil stainless steel wire is currently in use.

Although Teflon is presently being used as a liner, some experience has been obtained with other liner materials. The use of Delrin liners has resulted in cleaner driven-tube operation and, perhaps, in better performance. Unfortunately, the Delrin liners have a tendency to shatter. Wound-glass-filament liners give an increase in performance and are stronger and more durable than Teflon. However, removal of the ablation products which coat the driven tube requires a strong acid solution; hence, the use of these filament liners is undesirable. Further liner development is in progress.

The diaphragm is made from a 0.044-in. sheet of 321 stainless steel. The diaphragm is scribed approximately one-third of its depth, the scribe marks forming an "X" with the corners of the square. Static tests indicate that these diaphragms break at approximately 6500 psi. The driver pressure is of the order of 15,000 to 20,000 psi after the discharge. The present arrangement provides good opening characteristics for the diaphragm. From a photocell sighted along the axis of the tube, it was found that

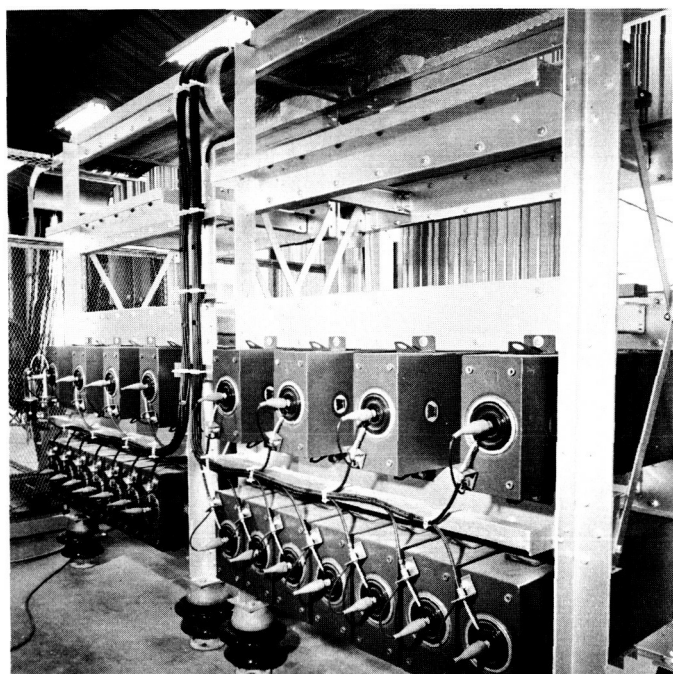


Fig. 4. Capacitor bank

the diaphragm begins to open about 80 μsec after the initiation of the discharge and is completely open approximately 200 μsec after the start of the discharge. Measurements described in Section II-C show that the electrical discharge is essentially completed in 50 to 60 μsec , providing a reasonably uniform slug of high-temperature, high-pressure gas behind the diaphragm.

C. Capacitor Bank

The capacitor room is shown in Fig. 4. The present bank has a capacity of 120,000 j, with a charging voltage of 20,000 v. The entire electrical system has been designed for 300,000 j, and provision has been made to expand the capacitor bank should this capacity be desired. Each of the 42 capacitors is rated at 14.5 μf . As indicated in Fig. 2, each of the capacitors is individually connected by a cable to the collector ring, where the electrical system is grounded. Since this is the only ground in the system, troublesome ground loops are eliminated. A gravity relay, a high-voltage vacuum switch, a ground switch, and a bank of discharge resistors complete the electrical system.

To determine the electrical characteristics of the capacitor bank, one of the capacitors is instrumented with a small current shunt and a capacitor voltage divider. Figure 5 shows typical voltage and amperage characteristics of the bank during discharge.

The control console for the bank (Fig. 6) is located in a separate control room. Controls for charging and discharging the bank, remote oscilloscope and camera controls, and remote valving for the vacuum system are

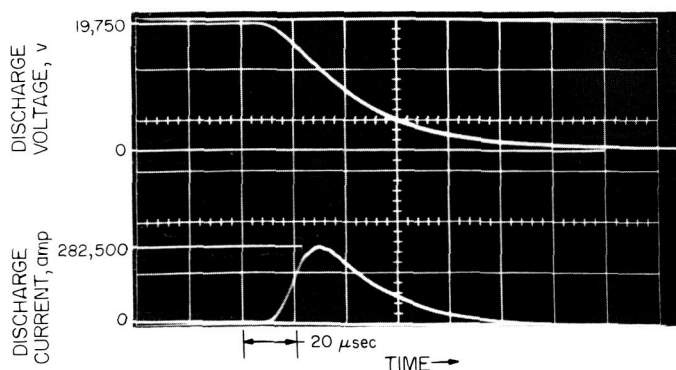


Fig. 5. Voltage and amperage characteristics of capacitor bank

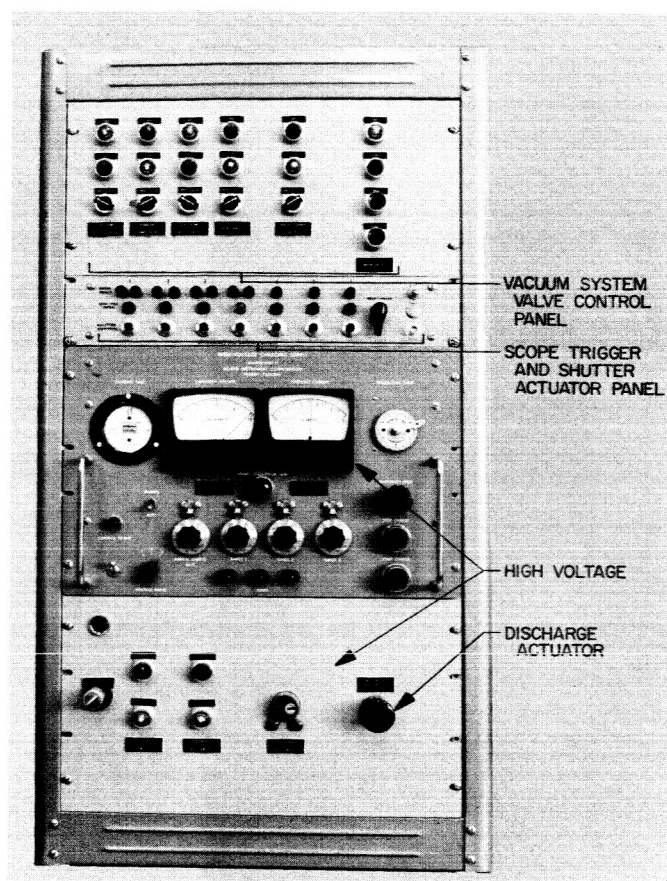


Fig. 6. Control console

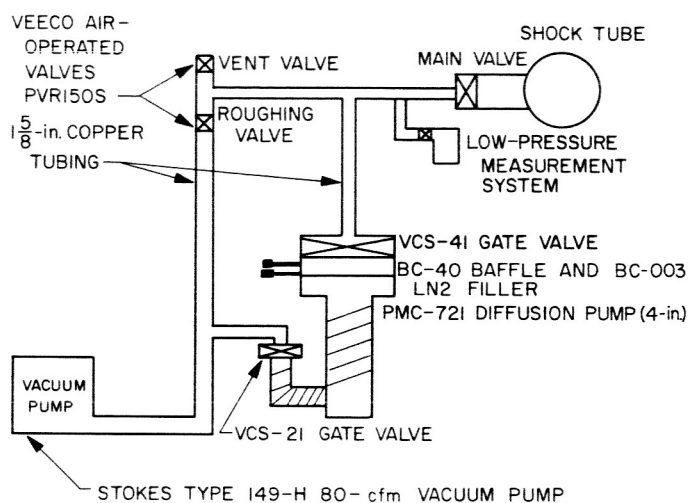


Fig. 7. Vacuum system schematic

indicated in the Figure. A detailed explanation of this console is given in Section IV.

D. Vacuum System

A schematic of the vacuum system is shown in Fig. 7. The system is capable of pump-down pressures less than 5×10^{-5} mm Hg. The main valve, designed specifically for the 6-in. shock tube, is a high-pressure form-fitting valve. The present leak rate for the driven tube and vacuum system is less than $1 \mu/\text{hr}$.

III. BASIC INSTRUMENTATION

Two fundamental measurements in shock tube tests are the initial pressure and the shock speed. With these two measurements and the conservation equations for a shock wave, it is possible to calculate the equilibrium thermodynamic state of shock-heated gas.

The generation of a uniform high-temperature slug of gas is, indeed, the purpose of a shock tube. A necessary part of the evaluation of shock tube performance is the instrumentation that demonstrates the existence of the uniform gas slug. This Section describes the basic instrumentation of initial-pressure and shock-speed measurement, and also the functions of the instrumentation ports and model support. In Section V, measurements used to determine the quality of the gas slug are discussed.

A. Initial-Pressure System (Driven Tube)

The initial pressure in the driven tube is determined by a system designed to measure pressure in the range of 0 to 15 mm Hg (absolute). The pressure transducer used is a differential-type Statham strain gage, with a vacuum of about $10\ \mu$ on the reference side of the transducer. An excitation voltage of approximately 2 to 3 v is applied across the gage, and its output is displayed on a digital voltmeter. The transducer, vacuum system, digital voltmeter, and associated power supplies are contained in a cabinet, as shown in Fig. 8.

The transducer is calibrated in the 0- to 10-mm range by means of a micromanometer (shown in Fig. 8) utilizing DC-200 oil and having a pressure range of 0 to 12 mm. This manometer, a primary standard, is fully described in Ref. 3. The accuracy of the calibrated transducer is $\pm 5\ \mu$ in the 0- to 1-mm range, which has been the range of utilization of the system.

A more accurate transducer in the range of 0 to 2.5 mm Hg is also used with a least count of $\pm 1\ \mu$.

B. Shock-Speed Determination

The intense radiation at the shock front is utilized to measure the shock speed. Three pairs of photomultipliers are placed perpendicular to the axis of the tube, the units of each pair being 1 ft apart. The radiation of

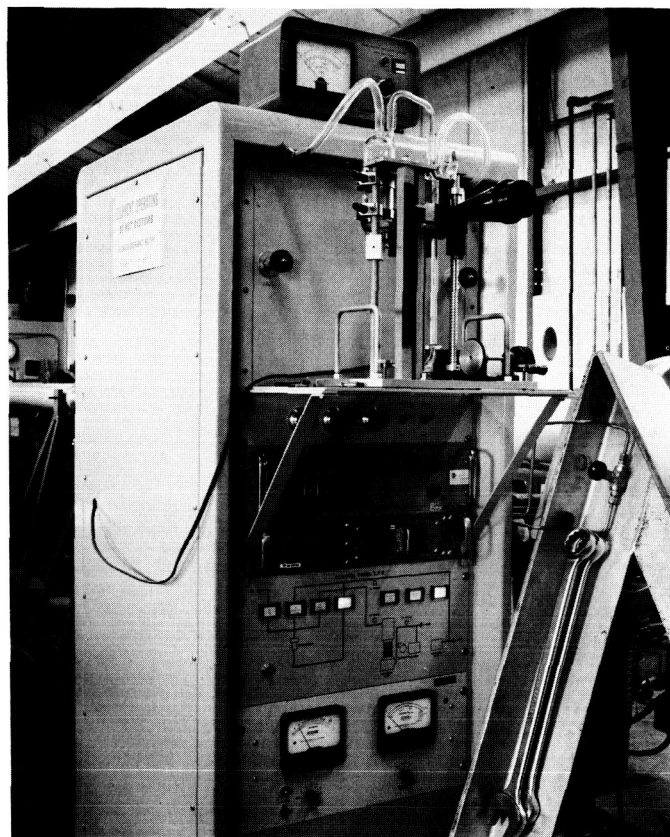


Fig. 8. Low-pressure measuring system

the photocells is collimated through four 0.006-in. slits, yielding a passage time of a fraction of a microsecond. Because of the change of radiation intensity, each photocell sees (1) the arrival of the shock, (2) the test gas or test time, (3) the contact surface, and (4) the arrival of the expansion wave. Figure 9 shows a typical photomultiplier record of the flow history. The typical nonequilibrium overshoot as the shock arrives is clearly indicated. The measured time between the two nonequilibrium peaks is used to obtain the shock speed, and the flat plateau after the overshoot is interpreted as the equilibrium test time. The arrival of the driver gas behind the contact surface is indicated by the sudden increase in intensity. The subsequent decrease in intensity is believed to be due to the arrival of the expansion wave. The photomultiplier records supply not only the shock speed as a function of distance along the tube, but also useful information as to the growth of test time along the tube and the character of the test slug. These data are more fully discussed in Section V.

Figure 10 shows a block diagram of the shock-speed measuring system. The output of the photocells is fed into a raster system. Since only the arrival of the shock is needed for shock-speed determination, the remainder of the signal is masked by a noise gate, and a uniform pulse is formed. Pulses from all the stations are then mixed and

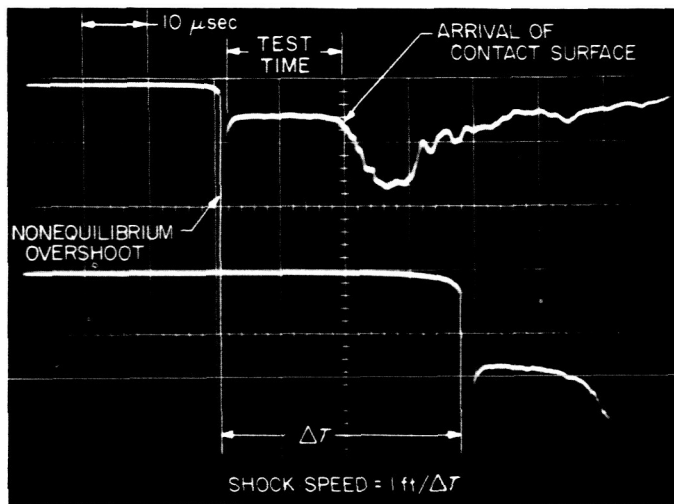


Fig. 9. Photomultiplier trace

fed into the Y axis of an oscilloscope, together with a sawtooth input which drives the signal vertically. A raster generator feeds triangle pulses into the X axis and time-mark pulses into the Z (intensity modulation) axis. A sweep length of 80 to 100 cm is produced, as opposed to the conventional sweep length of 10 cm. The crystal markers are placed 1 cm apart, and the sweep time can be chosen by varying marker, triangle, and sawtooth frequencies. Typically, markers occur at 5- or 10-μsec intervals, giving a total sweep time of several hundred microseconds. A typical raster trace is shown in Fig. 11.

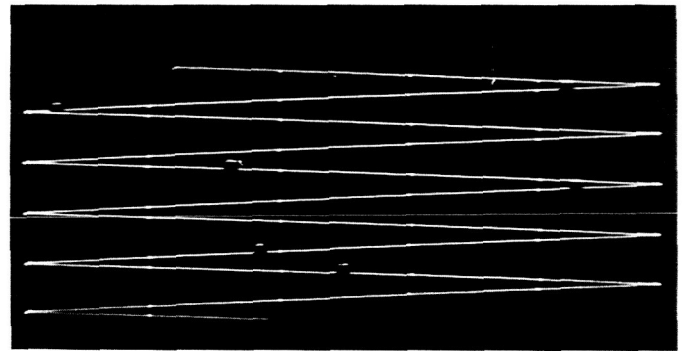


Fig. 11. Raster trace

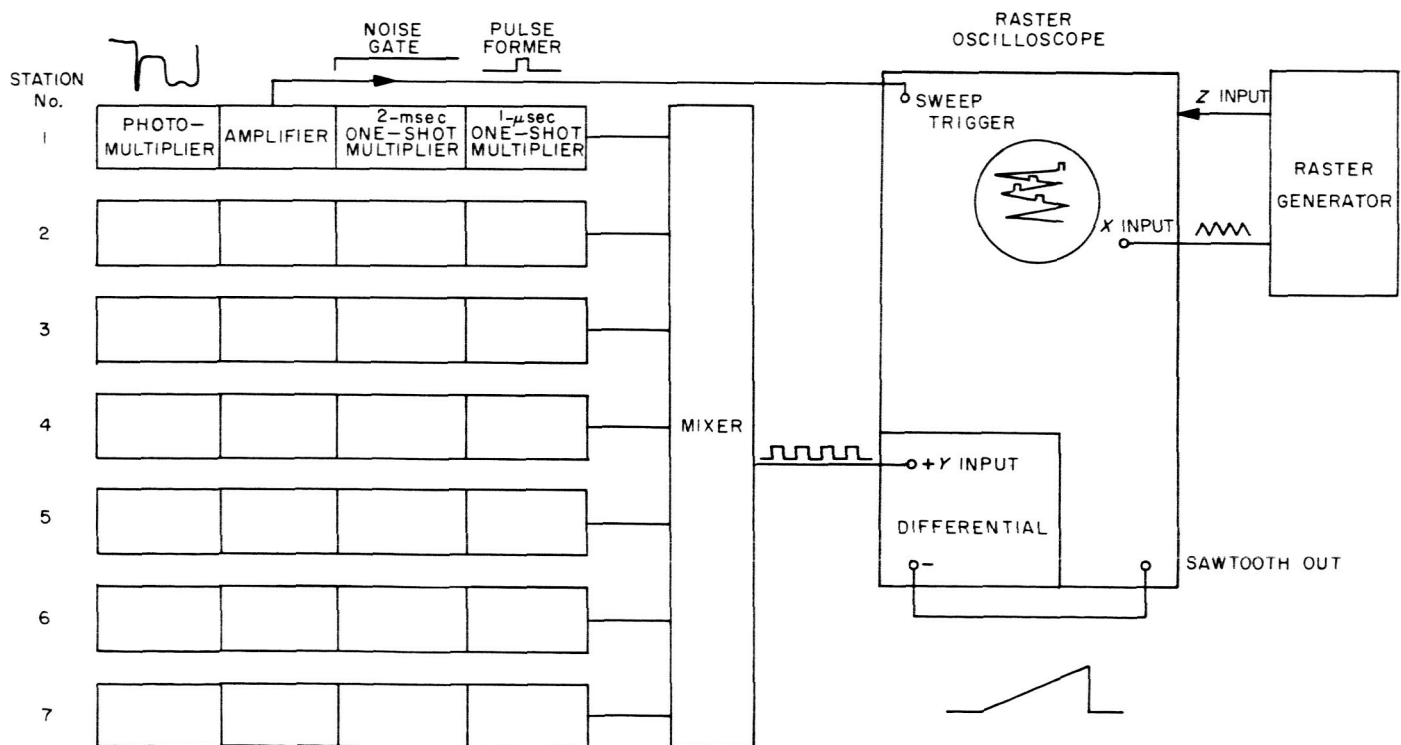


Fig. 10. Block diagram of shock-speed measuring system

Here, the total time history of the shock as it travels the length of the tube is recorded, and shock-speed and attenuation data can be obtained directly from this trace.

In addition to the photomultiplier determination of shock speed, the velocity of the shock was measured by a Kistler pressure gage. Within the accuracy of the measurements, the pressure-determined shock speed agreed with that determined by the photomultipliers. The arrival of the expansion surface, as indicated by the pressure transducer, also agreed with photomultiplier data.

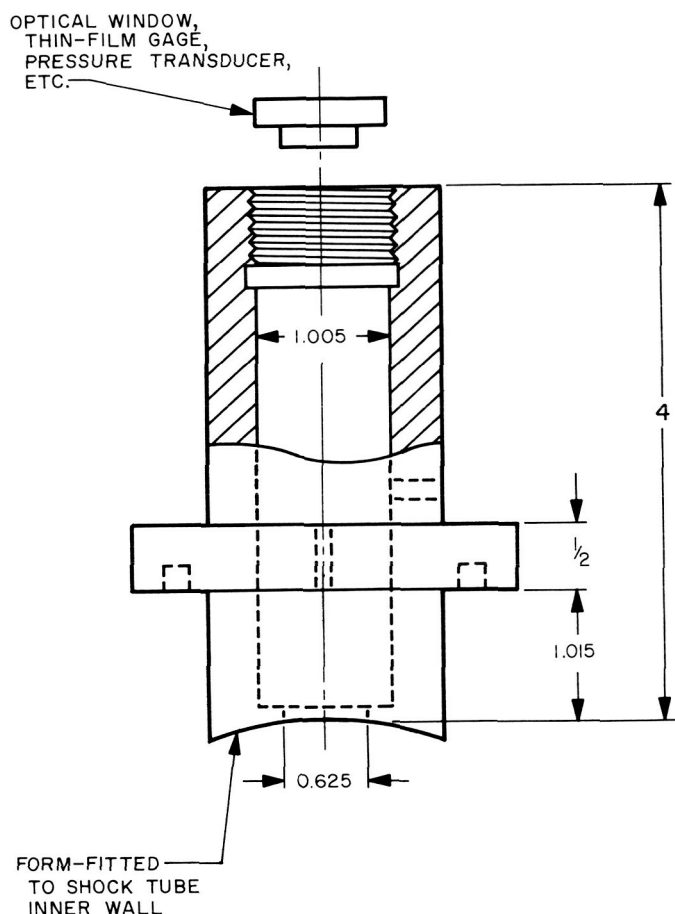


Fig. 12. Sketch of instrument port

C. Model Support and Instrument Ports

In addition to the two basic measurements of initial pressure and shock speed, measurements of the test gas must be performed. Sidewall measurements are obtained by utilizing instrument ports, as shown in Fig. 12. With this arrangement, optical, pressure, and thin-film measurements can be made with interchangeable inserts.

The model support is shown in Fig. 13. Attached to the support is a 1-in. calorimeter model that has been used in the determination of convective heat transfer in planetary atmospheres. This support has also been used for a flat-face radiation model, employed to determine the total radiant heat transfer from planetary atmospheres.

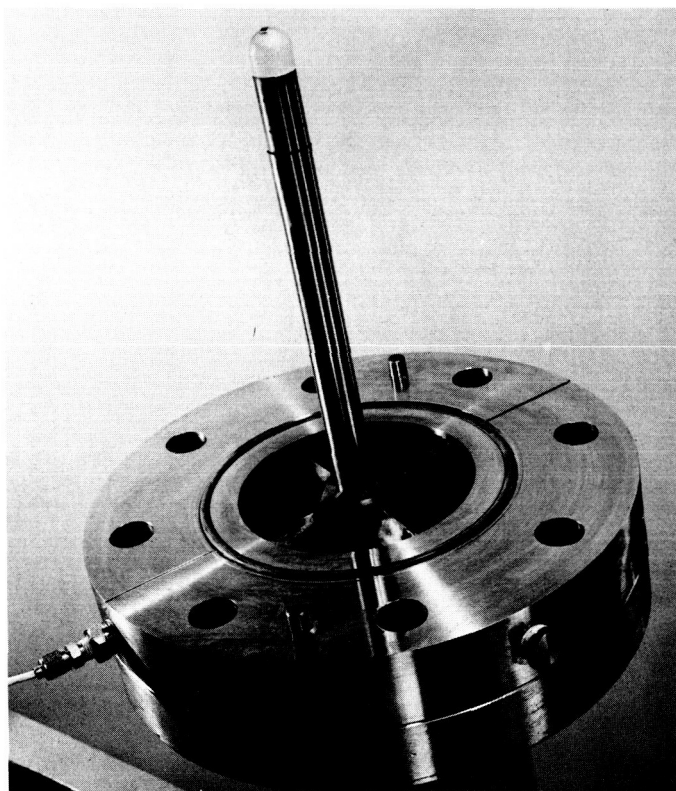


Fig. 13. Model support

IV. OPERATION

The capacitor bank is located in an enclosed area which is outside the general working area. The control area is enclosed by a strong wall, composed of two layers of $\frac{1}{4}$ -in. steel plate and two layers of $\frac{1}{2}$ -in. plywood. Before the capacitor bank is charged, all personnel are assembled in the control area. To ensure that the capacitor bank area and the shock tube area are cleared, a key-interlock system was installed. The capacitor bank cannot be charged until the correct key is inserted in the control panel. This ensures several safety procedures: to obtain the proper key, the door to the shock tube area must be locked, the door to the capacitor room must be locked, and a safety switch must be opened. After firing, before the shock tube area or the capacitor bank area can be entered, the capacitors must be discharged through a bank of resistors, and all capacitors must be physically grounded by closing the safety ground switch. Only after completion of this procedure can the shock tube area be entered.

The control panel shown in Fig. 6 is located within the control area. It consists of three units: (1) the upper unit, containing the controls for various valves which are part of the vacuum system; (2) the second unit from the top, comprising the scope trigger and shutter actuator panel, which allow the operator to reset the sweeps and open the shutters of the oscilloscopes being used in the shock tube area; and (3) the last two panels, constituting the controls for the high-voltage charging unit and the discharge actuator.

In the bottom panel (Fig. 6), the key insert for the key-interlock system can be seen. To the right of the insert is the discharge actuator, or *fire* button; this mechanism activates the solenoid which closes the circuit and discharges the capacitor bank. The remote operation of the shock tube from this control panel ensures maximum safety for operating personnel.

V. PERFORMANCE AND EVALUATION

In keeping with the need to use a driver gas having as low a molecular weight as is practicable, the gas employed is helium. The real-gas equilibrium conditions in the driver have been calculated (Ref. 4) as a function of total energy input, using a Mollier Diagram for helium (Ref. 5). The pressure P_4 , temperature T_4 , and the ratio between the sound-speed of helium a_4 and the sound-speed of air a_1 are plotted as functions of energy input (j/cm^3) in Figs. 14, 15, and 16. These values for the thermodynamic state behind the diaphragm are used in the performance calculations of the shock tube.

Some typical measured values of shock speed V_s as a function of energy input $\Delta E/V$ (Ref. 6) are shown in Fig. 17. An empirical correction to the sound-speed of the driver gas (helium) has been made to account for the inclusion of liner ablation products in the gas (Ref. 1). This correction changes the sound-speed to a value which represents about 77% of the theoretical value. The maximum shock speed measured with useful test time has

been about 32,000 fps into 250 μ Hg in the 6-in. driven tube at a length/diameter (L/D) ratio of 71. These measurements were made in a 9% CO_2 , 1% A, 90% N_2 mixture. The test time was approximately 12 μsec . At a lower initial pressure, it is clear that shock velocities of 35,000 fps with useful test times of about 7 to 8 μsec are obtainable. In the electrical hypervelocity shock tube, the ultimate shock velocity with a still useful test time would be, perhaps, of the order of 40,000 fps. Contrary to what one might think from theoretical considerations, higher initial driver pressures ($P_4 \approx 225$ psi) have given higher shock speeds for the same energy input.

Shock attenuation as a function of distance from the diaphragm is shown in Fig. 18, where a comparison is made with the AVCO Corporation data from a similar shock tube (Ref. 1). The peak attenuation rate is obtained in the first 28 ft of the driven tube. The data indicate that, at the higher initial driver pressures ($P_4 \approx 225$ psi), the attenuation is smaller.

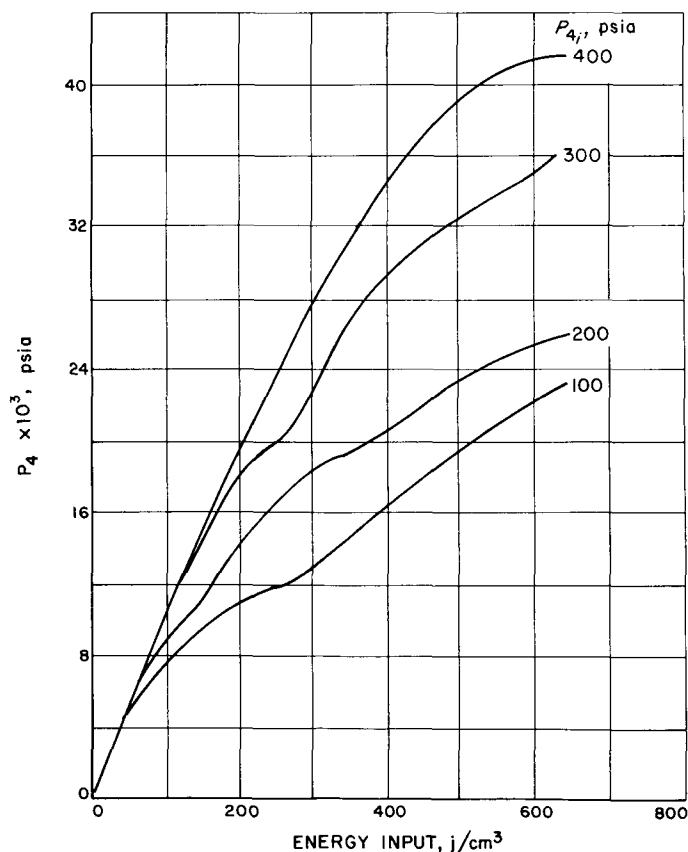


Fig. 14. Driver pressure vs energy input

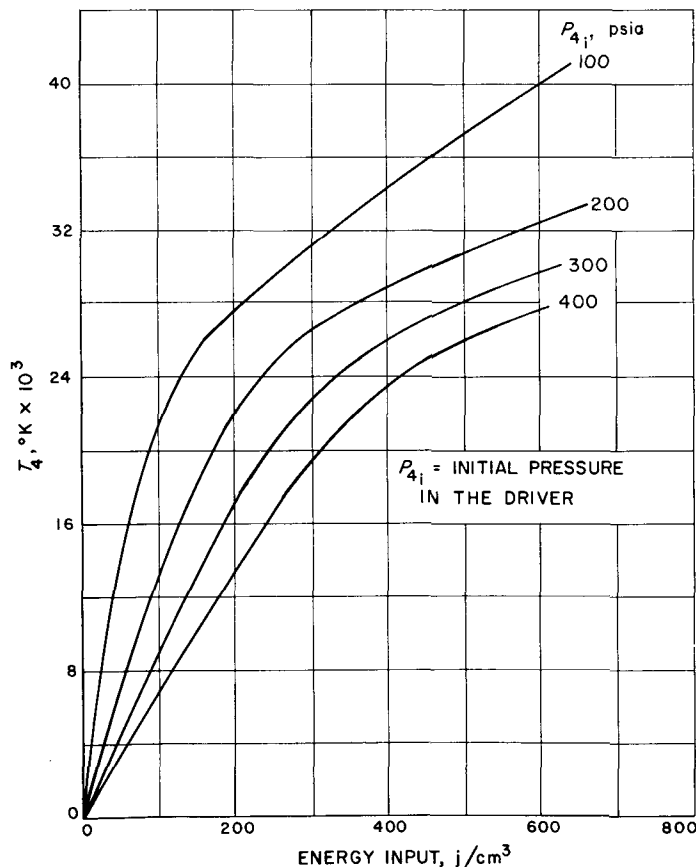


Fig. 15. Driver temperature vs energy input

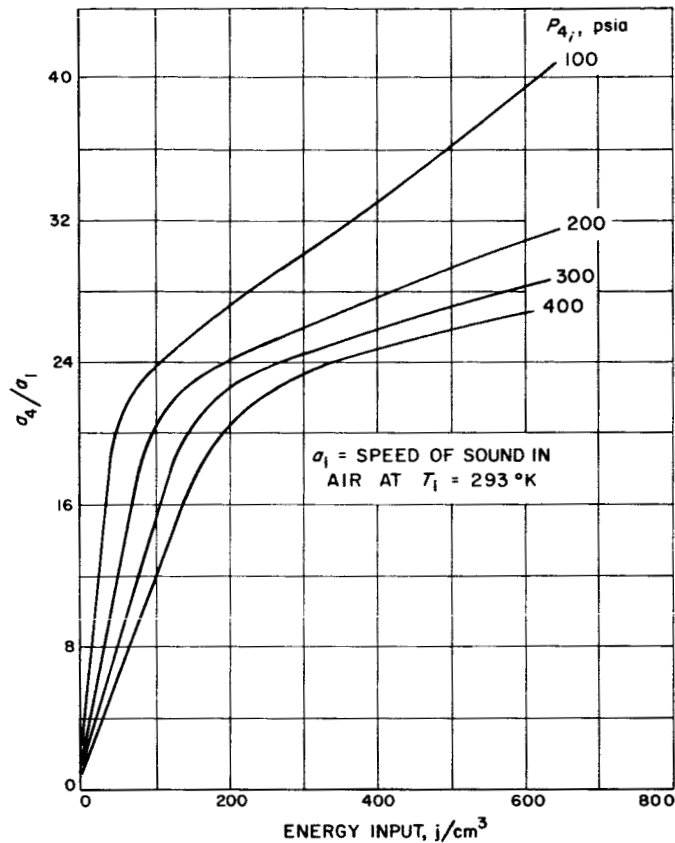


Fig. 16. Sound-speed ratio vs energy input

In Figs. 19 and 20, some measured test times are plotted for initial driven tube pressures P_i of 0.250 and 1 mm Hg. The test times are given as measured at an L/D value of 54.5, in order to make a valid comparison with previous data reported in Ref. 1. Again, it is evident that higher driver pressures (~ 250 psi) give better test times, in general.

In an effort to verify the existence of a straight shock and a uniform test slug, pictures of the shock wave were taken with an image-converter camera. A 6-in. Pyrex insert allows a picture of the complete shock in the 6-in. tube. The resulting photographs (Fig. 21) show a straight shock, as well as a uniform test slug. A bright region at the front of the shock is due either to impurity radiation or to nonequilibrium radiation. The turbulence at the contact surface is characteristic of high-velocity shocks. In some cases, this turbulent region extends throughout the entire test slug, so that no useful test time is obtained.

A further indication of a good test gas is given by the output of photomultipliers, as shown in Fig. 9. The flat plateau indicates a good test slug. Where the photographs

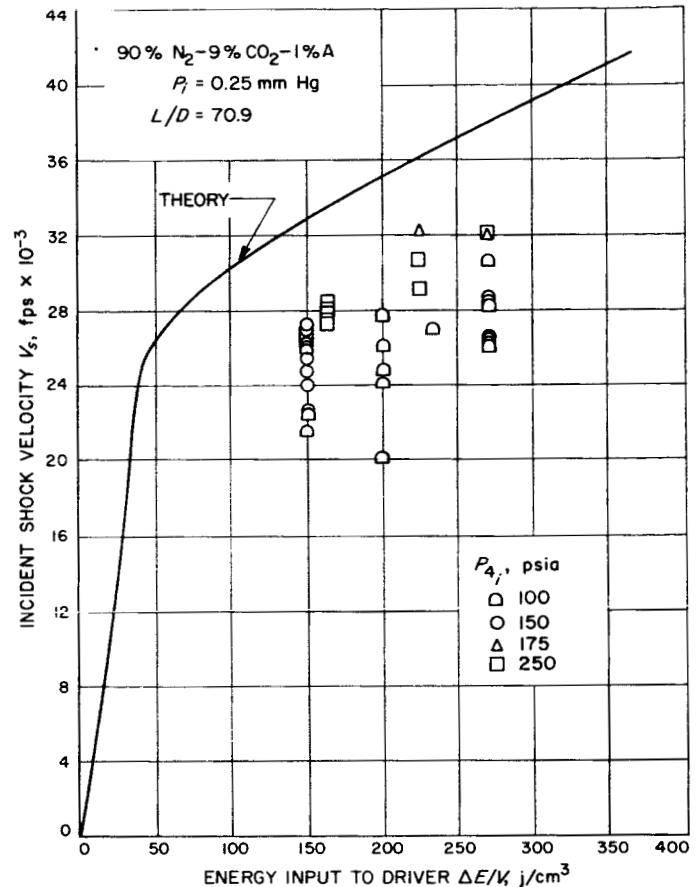


Fig. 17. Shock speed vs energy input

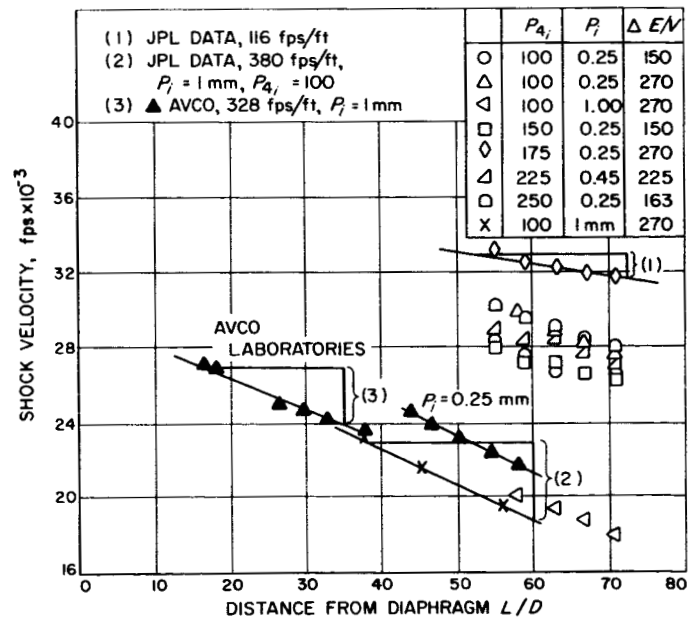
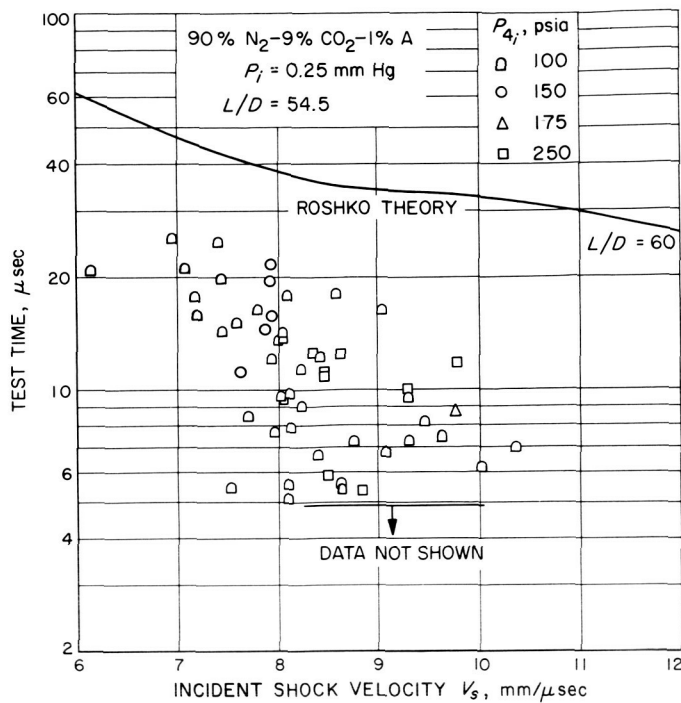


Fig. 18. Shock-speed attenuation

Fig. 19. Test time vs shock speed (250 μ i)

have indicated an extended turbulent region or a non-planar shock, the photomultiplier output shows a distinct slope. When model tests are conducted, such as studies of convective heat transfer or total radiant heat transfer, the quality of the test slug is further checked by means of a monitoring photocell collimated in front of the model. A good test-gas sample is indicated by a flat plateau similar to that shown in the previous photocell output.

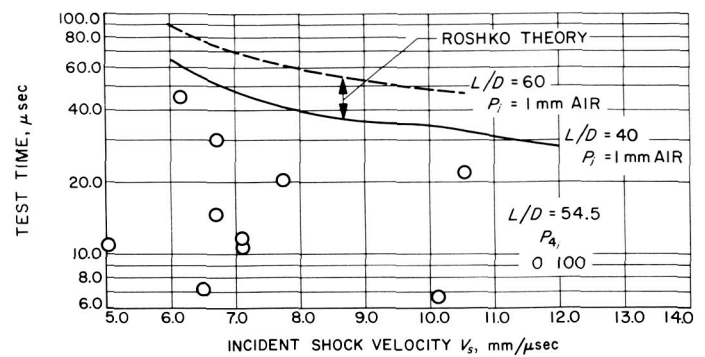


Fig. 20. Test time vs shock speed (1 mm)

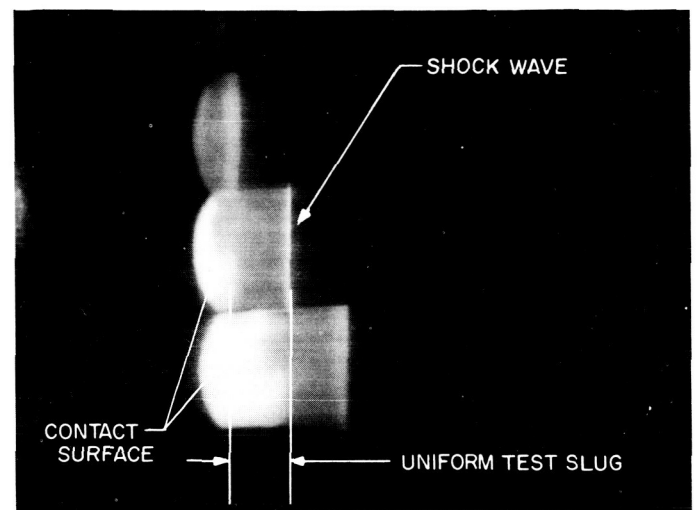


Fig. 21. Image-converter-camera photograph of shock wave

VI. SUMMARY

The electrical shock tube has the capability of simulating entry velocities up to 45,000 fps. This is adequate for Venus missions and more than adequate for Mars missions. The shock tube has already produced useful information on convective and radiative heat transfer in planetary atmospheres; these data have been summarized in Refs. 7, 8, and 9, and will be discussed more fully in a future technical paper.¹ Active investigations of radiant gases are now being conducted on simulated planetary

atmospheres. The engineering information obtained in these studies will be useful in determining design specifications of the spacecraft for planetary missions to Mars and Venus.

¹Thomas, G. M., and Menard, W. A., *Experimental Measurements of Nonequilibrium and Equilibrium Radiation from Planetary Atmospheres*, to be presented at the Re-entry Physics Session of the AIAA Entry Technology Conference, Williamsburg, Virginia, October 12-19, 1964.

REFERENCES

1. Rose, P. H., and Camm, J. C., *Electric Shock Tube for High Velocity Simulation*, Report 136, AVCO-Everett Research Laboratory, Everett, Massachusetts, July 1962.
2. Warren, W. R., Rogers, D. A., and Harris, C. J., *The Development of an Electrically Heated Shock Driven Test Facility*, Report R62SD37, Space Sciences Laboratory, Missile and Space Division, General Electric Company, Philadelphia, Pennsylvania, April 1962.
3. Kendall, J. M., *The Design and Performance of Precision Oil Micromanometers*, NAVORD Report 6803, U. S. Naval Ordnance Laboratory, White Oak, Maryland, June 29, 1961.
4. Collins, D. J., and Babineaux, T. L., "Real Gas Performance of Helium Drivers," *AIAA Journal*, Vol. 1, No. 6, June 1963.
5. Lick, W. J., and Emmons, H. W., *Thermodynamic Properties of Helium to 50,000°K*, Harvard University Press, Cambridge, Massachusetts, 1962.
6. Babineaux, T. L., "Shock Tube Laboratory," *Space Programs Summary No. 37-21*, Vol. IV, p. 82, Jet Propulsion Laboratory, Pasadena, California, June 20, 1963.
7. Collins, D. J., "Convective Heat Transfer in Carbon Dioxide," *Space Programs Summary No. 37-24*, Vol. IV, p. 78, December 31, 1963.
8. Collins, D. J., and Spiegel, J. M., "The Effect of Gage Material on Convective Heat Transfer," *AIAA Journal*, Vol. 2, No. 5, May 1964.
9. Thomas, G. M., "Experimental Radiation Measurement Techniques," *Space Programs Summary No. 37-24*, Vol. IV, p. 78, December 31, 1963.

ACKNOWLEDGMENTS

The authors wish to acknowledge the considerable assistance of the General Electric Company and the AVCO Corporation in the construction of the hypervelocity shock tube. Among the numerous Laboratory personnel who contributed greatly to the development of the facility, the following deserve particular mention: R. M. Noble, for the electrical design of the capacitor bank and control system; C. M. Berdahl and R. G. Harrison, Jr., for the instrumentation; E. W. Noller, for mechanical design support; and R. H. Lee, for the construction of the vacuum system and the mechanical assembly of the shock tube and affiliated systems.